[1]S. Bashkin, Nucl. Instr. Method 28, 88 (1964).

[2]*Beam-Foil Spectroscopy*, edited by S. Bashkin (Gordon and Breach, New York, 1968); I. Martinson, J. Bromander, and H. G. Berry, Nucl. Instr. Methods 90, (1970).

[3]C. H. Liu, S. Bashkin, W. S. Bickel, and T. Hadeishi, Phys. Rev. Letters 26, 222 (1971).

[4]C. Moore, *Atomic Energy Levels*, Vol. 1, Natl. Bur. Std. (U.S.) Circ. No. 467 (U.S. GPO, Washington, DC, 1949).

[5]C. H. Liu and D. A. Church, Phys. Letters 35A, 407 (1971).

[6]J. B. Green and J. A. Peoples, Jr., Phys. Rev. 54, 602 (1938).

[7]T. Hadeishi, Phys. Rev. 162, 16 (1967).

[8]B. Fastrup, P. Hvelplund, and C. A. Sautter, Kgl. Danske Videnskab. Selskab, Mat. Fys. Medd. 35, No. 10, 1 (1966).

[9]J. O. Stoner, Jr., J. Appl. Phys. 40, 707 (1969).

[10]J. H. Brand, C. L. Cocke, B. Curnutte, and C. Swenson, Nucl. Instr. Methods 90, 63 (1970).

[11]A. R. Striganov and N. S. Sventitskii, *Tables of Spectral Lines of Neutral and Ionized Atoms* (IFI/Plenum Data Corporation, New York, 1968).

[12]J. Z. Klose, J. Opt. Soc. Am. 58, 1509 (1968).

[13]R. I. Rudko and C. L. Tang, J. Appl. Phys. 38, 4731 (1967).

[14]D. A. Church, M. Druetta, and C. H. Liu, Phys. Rev. Letters 27, 1763 (1971).

[15]A discussion of such an effect, and its implications for Hanle-effect measurement, is given by R. K. Wangsness, Phys. Rev. A 3, 1275 (1971).

PHYSICAL REVIEW A VOLUME 5, NUMBER 3 MARCH 1972

Hyperfine Structure of Excited States and Quadrupole Moment of Ne^{21} Using Laser-Induced Line-Narrowing Techniques*

T. W. Ducas, M. S. Feld, L. W. Ryan, Jr., N. Skribanowitz, and A. Javan
Department of Physics, Massachusetts Institute of Technology, Cambridge, Massachusetts 02139
(Received 17 May 1971)

Optical hyperfine structure in Ne^{21} has been observed using laser-induced line-narrowing techniques. The output from a long stabilized single-mode 1.15-μ He-Ne laser is focused into an external sample cell containing Ne^{21}. The laser field resonates with the Ne^{21} 1.15-μ transition causing changes in the level populations over a narrow velocity range. Viewed along the laser axis, these population changes appear as narrow "change signals" superposed on the Doppler background of the spontaneous emission of the coupled 6096-Å transition. Analysis of the spectrum of these change signals, emitted parallel and antiparallel to the laser-field propagation direction, gives values for the hyperfine A constants for the three levels involved. These constants are analyzed by means of theoretical expressions wherein $\langle 1/r^3\rangle$ of the $2p$ hole is the single important parameter. Combining the resulting value of $\langle 1/r^3\rangle_{2p\,\mathrm{hole}}$ for the $1s_4$ level with a previous measurement of $B(1s_5)$ gives a value of $Q(1s) = (0.093 \pm 0.002)$ b, in agreement with an earlier less-accurate value. In addition, the $Ne^{20,21,22}$ isotope shifts are measured at 1.15 μ and 6096 Å.

INTRODUCTION

Laser-induced line-narrowing spectroscopy[1] has been used to observe optical hyperfine structure in Ne^{21}. This technique represents an advance in several ways over other methods of investigating hyperfine and other closely spaced structure in Doppler-broadened systems. The best conventional optical spectrometers, even if not instrument limited in resolution, are unable to resolve hyperfine transitions whose structure is buried within the Doppler profile. Atomic-beam studies in rare gases eliminate the Doppler effect, but have been generally limited to metastable levels, the only states with hyperfine structure that have lifetimes sufficiently long for beam techniques. Furthermore, ordinary beam techniques are incapable of measuring isotope shifts.

In the present approach, an optical technique[2-5] is used in which the Doppler width is effectively eliminated by laser-induced velocity selection. Measurements of the narrowed spectral lines have yielded values for the isotope shifts of $Ne^{20,21,22}$ at 1.15 μ and 6096 Å and hyperfine constants of Ne^{21}, which lead to an accurate value for the Ne^{21} quadrupole moment.

The level scheme under study (Fig. 1) consists of the hyperfine sublevels of the $2s_2$, $2p_4$, and $1s_4$ fine-structure levels[6] of Ne^{21} (nuclear spin $I = \frac{3}{2}$), which form the 1.15-μ ($2s_2 - 2p_4$) and 6096-Å ($2p_4 - 1s_4$) cascade transitions. The magnetic dipole and electric quadrupole hyperfine interactions split each fine-structure level (angular momentum J) into a number of hyperfine components, of energy

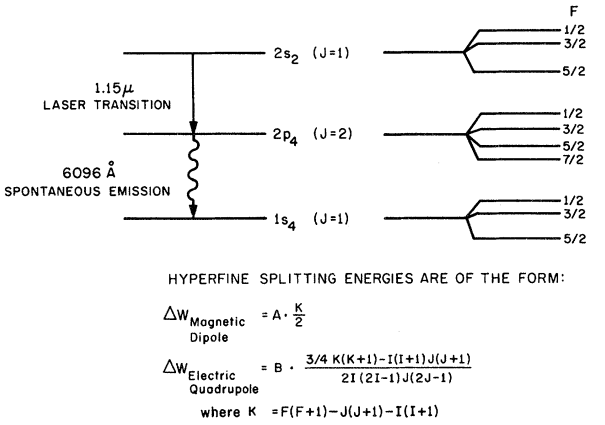

FIG. 1. Hyperfine splitting of $1s_4$, $2p_4$, $2s_2$ levels in Ne^{21}.

$$W_F = W_J + A\tfrac{1}{2}K + B\,\frac{\frac{3}{4}K(K+1) - I(I+1)\,J(J+1)}{2I(2I-1)J(2J-1)}, \quad (1)$$

where $K = F(F+1) - I(I+1) - J(J+1)$ and F, the total angular momentum, can take on the values: $F = I+J$, $I+J-1, \ldots, |I-J|$. W_F is the total energy of the hyperfine level, W_J is the energy of the fine-structure level; A and B are the magnetic dipole and electric quadrupole interaction constants of level J, respectively.

LASER-INDUCED LINE-NARROWING EFFECT

A comprehensive treatment of the laser-induced line-narrowing effect is given in Ref. 1. The following simplified discussion will provide a sufficient background for an understanding of the present experiment. Let us consider a particular coupled three-level system in Ne^{21} consisting of a pair of hyperfine transitions, one at 6096 Å and one at 1.15 μ, which share a common level. If a 1.15-μ traveling-wave laser field is incident upon a sample of Ne^{21}, the atoms over a narrow range of axial velocities which are Doppler shifted into resonance with the applied field coupled most strongly to it. This causes selective changes in the level populations over the narrow velocity range. These changes have a Lorentzian line shape centered about $v = (\Omega_L - \omega_2)/k_2$, and the velocity range is $\Delta v \sim \gamma/k_2$, where Ω_L is the frequency of the laser, ω_2 is the atomic center frequency of the 1.15-μ hyperfine transition, k_2 is the corresponding propagation constant, and γ is the homogeneous linewidth of the laser transition.

This change in the velocity distribution manifests itself in a change of intensity with a Lorentzian line shape (change signal) in the coupled 6096-Å fluorescence over a narrow section of the Doppler profile emitted along the axis of propagation of the laser field (Fig. 2). The peak of this spontaneous emission signal in the forward direction (i.e., parallel to the propagation vector of the laser field $\vec{k}_L$) occurs at $\Omega_F = \omega_1 + k_1 v$, and the backward (antiparallel) change signal occurs at $\Omega_B = \omega_1 - k_1 v$; where ω_1 is the atomic center frequency of the coupled 6096-Å transition.[7]

The locations of these change signals can be rewritten simply as

$$\Omega_F = \omega_1 + (\Omega_L - \omega_2)\,\omega_1/\omega_2, \quad (2a)$$

$$\Omega_B = \omega_1 - (\Omega_L - \omega_2)\,\omega_1/\omega_2\,. \quad (2b)$$

Thus, the separation between change signals due to the pair (j, k) of closely spaced three-level systems is given by

$$\Omega_F(j) - \Omega_F(k) = [\omega_1(j) - \omega_1(k)] - [\omega_2(j) - \omega_2(k)]\,\omega_1/\omega_2, \quad (3a)$$

$$\Omega_B(j) - \Omega_B(k) = [\omega_1(j) - \omega_1(k)] + [\omega_2(j) - \omega_2(k)]\,\omega_1/\omega_2\,. \quad (3b)$$

The hyperfine interactions in Ne^{21}, which produce 18 such three-level systems, can be analyzed from Eqs. (3). Note that forward and backward patterns contain information on the hfs of both 1.15-μ and 6096-Å transitions. Separate observation of forward and backward signals[5] provides two distinct patterns which must be fit by a single set of parameters. These parameters, the hyperfine A and B constants for each of the three levels, can be extracted from the separations between the features of the spectrum. The fact that the relative positions of the change signals are independent of laser tuning [Eq. (3)] greatly simplifies the analysis.

The complete theoretical expression describing the laser-induced change signals is given in the

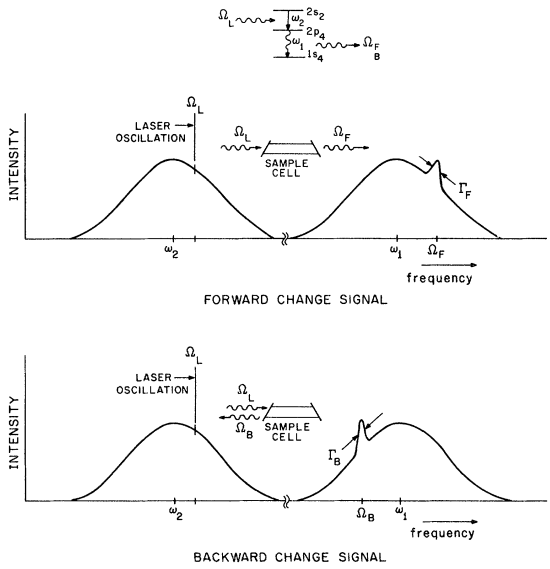

FIG. 2. Change signals produced in laser-induced line narrowing.

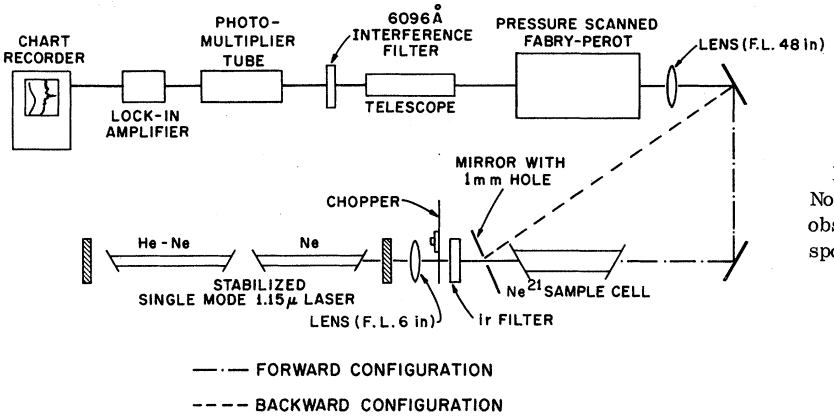

FIG. 3. Experimental arrangement. Note the different configurations for observing forward and backward 6096-Å spontaneous emission.

Appendix.

EXPERIMENTAL ARRANGEMENT

The experimental setup is shown in Fig. 3. An intense single-mode[8,9] 1.15-μ He-Ne laser (see below) is locked to the resonance of a stable passive Fabry-Perot interferometer by standard methods. The laser output beam is focused into an external sample cell containing Ne^{21} at a low pressure (~0.1 Torr). The 6096-Å spontaneous emission from the sample cell, emitted in either the forward or backward[10] direction, is analyzed using a pressure-scanned Fabry-Perot interferometer with a free spectral range of 4090 MHz and a finesse of 40. The entire apparatus is shock mounted to reduce vibration effects. Linear scanning is achieved with a system of capillary tubes[11] bleeding dry air into a cannister containing the interferometer. A chopper, placed between the laser and the sample cell, enables us to use a lock-in amplifier to subtract off the spontaneous emission background and improve the signal-to-noise ratio.

In this experiment it is essential to have the laser operate in a single mode, since each extra mode would produce an additional set of change signals. It is also important to maximize the power in this mode since the sizes of the change signals are essentially proportional to the laser-field intensity. This is particularly critical in this experiment because the sample cell is outside the laser resonator. Neither short laser cavities nor conventional Michelson mode-selection techniques can satisfy the single-mode power requirement. We have employed instead the following arrangement.[8,9]

Within the laser resonator (length 1.6 m) along with the He-Ne amplifier cell (total pressure ~2 Torr) we have placed an absorber cell filled with neon at a low pressure (~0.2 Torr). The cells are of comparable length and the small signal gain of the amplifier is several times as large as the loss of the absorber. While the linear gain of the system is dominated by the amplifier cell, the absorber, which saturates more readily, contributes appreciably to the saturation behavior. The result is that the system is driven into the strong-coupling regime, where the modes compete heavily with one another. Thus, laser oscillation at one mode tends to suppress oscillation at other modes. The net result is a continuously tunable single-mode output with an appreciable fraction of the full power of multimode operation. In our experiment we were able to convert over 50% of the multimode power (9 modes) into a single mode.

HYPERFINE THEORY

The electronic configurations of excited states in neon consist of a $2p$ hole coupled to an excited electron surrounding closed shells. The wave functions of the resulting fine-structure (fs) energy levels, obtained from the fs energy splittings,[12] may be expressed in terms of an admixture of the appropriate LS wave functions.[13,14] The A and B interaction constants which determine the hyperfine spectrum [Eq. (1)] may be obtained from these wave functions, the nuclear dipole moment μ, and the nuclear quadrupole moment Q.[15] The resulting expressions for the A's and B's of the three levels of interest contain the coefficients of the LS wave functions and the parameters: μ; Q; $\langle 1/r^3 \rangle$ for the $2p$ hole; $\langle 1/r^3 \rangle$ for the $3p$ electron; and the contact terms a_{3s} and a_{4s} for the $3s$ and $4s$ states of the excited electron.

In a previous experiment[16] Grosof, Buck, Lichten, and Rabi measured the A and B constants of the $1s_5$ level of Ne^{21} to high (0.1%) accuracy. But since $\langle 1/r^3 \rangle_{2p\,\mathrm{hole}}$ can only be estimated to 10% accuracy, using the Fermi-Segre formula[15] and their measured value of $A(1s_5)$, their value of Q has this same uncertainty [$B(1s_5) \propto Q\langle 1/r^3 \rangle_{2p\,\mathrm{hole}}$].

We make use of the measured[16] values of $A(1s_5)$ and $B(1s_5)$ and of the known[17] value of μ to reduce the number of parameters in our theoretical description by three: Q is expressed in terms of $B(1s_5)$ and $\langle 1/r^3 \rangle_{2p\,\mathrm{hole}}$, and a_{3s} may be expressed

in terms of $A(1s_5)$ and $\langle 1/r^3\rangle_{2p\,\mathrm{hole}}$ (independent of the admixture of states for the $1s_5$ level). The remaining parameters are $\langle 1/r^3\rangle_{2p\,\mathrm{hole}}$, $\langle 1/r^3\rangle_{3p\,\mathrm{electron}}$, and a_{4s}. The contribution of the $3p$ electron to the hfs is negligible. Furthermore, the error in our estimate of a_{4s} (from the Fermi-Segre formula) produces only a small uncertainty in $A(2s_2)$. Thus, the hyperfine interaction constants are sensitive only to the $\langle 1/r^3\rangle_{2p\,\mathrm{hole}}$ parameter. In the following paragraphs we expand upon the preceding discussion and describe the particular calculations involved in obtaining expressions for the hyperfine constants.

In our analysis we use the wave functions of Vainshtein and Minaeva[14]:

$$\begin{aligned}
|2s_2\rangle &= -0.660\,|^3P_1\rangle + 0.752\,|^1P_1\rangle,\\
|2p_4\rangle &= 0.127\,|^3D_2\rangle - 0.309\,|^1D_2\rangle + 0.943\,|^3P_2\rangle,\\
|1s_4\rangle &= 0.964\,|^3P_1\rangle + 0.266\,|^1P_1\rangle,
\end{aligned} \tag{4}$$

where $|^{2S+1}L_J\rangle$ are wave functions in the LS representation. These wave functions have been derived from the fs energy splittings,[12] taking into account electrostatic, spin-orbit, spin-spin, and spin-other-orbit interactions.

The LS matrix elements for the magnetic dipole and electric quadrupole interactions for the p^5s and p^5p' configurations are given by Childs.[18,19] We use the nonrelativistic limit for these matrix elements since relativistic corrections are negligible ($<1\%$ for low-Z atoms such as neon). Combining these with Eqs. (4) we get the following expressions for the A and B interaction constants for the three levels of concern:

$$\begin{aligned}
A(2s_2) &= 1.352\,a_{2p\,\mathrm{hole}} + 0.460\,a_{4s},\\
B(2s_2) &= -0.139\,b_{2p\,\mathrm{hole}};\\
A(2p_4) &= 0.367\,a_{2p\,\mathrm{hole}} + 0.403\,a_{3p},\\
B(2p_4) &= 0.053\,b_{2p\,\mathrm{hole}} - 0.219\,b_{3p};\\
A(1s_4) &= 0.819\,a_{2p\,\mathrm{hole}} + 0.051\,a_{3s},\\
B(1s_4) &= 0.158\,b_{2p\,\mathrm{hole}};
\end{aligned} \tag{5}$$

with

$$\begin{aligned}
a_{np} &= (2\mu\mu_B/I)\,\langle 1/r^3\rangle_{np},\\
b_{np} &= e^2Q\langle 1/r^3\rangle_{np},
\end{aligned}$$

where μ_B is the Bohr magneton.

Now, if we employ the results of Grosof *et al.*[16] for the $1s_5$ level of Ne^{21}:

$$\begin{aligned}
A(1s_5) &= (-267.68 \pm 0.03)\ \mathrm{MHz},\\
B(1s_5) &= (-111.55 \pm 0.10)\ \mathrm{MHz},
\end{aligned}$$

and the fact that,[16] independent of the LS coefficients of the $1s_5$ wave function, we have

$$\begin{aligned}
A(1s_5) &= \tfrac{1}{4}\,a_{3s} + \tfrac{2}{5}\,a_{2p\,\mathrm{hole}},\\
B(1s_5) &= -\tfrac{2}{5}\,b_{2p\,\mathrm{hole}},
\end{aligned}$$

we can express our A and B constants in MHz in the following manner:

$$\begin{aligned}
A(2s_2) &= 0.460\,a_{4s} - 843.27R_h,\\
B(2s_2) &= -38.786;\\
A(2p_4) &= -228.78R_h - 251.39R_e,\\
B(2p_4) &= 14.898 - 61.191\,R_e/R_h;\\
A(1s_4) &= -54.639 - 459.74R_h,\\
B(1s_4) &= 43.940;
\end{aligned} \tag{6}$$

where

$$\begin{aligned}
\langle 1/r^3\rangle_{2p\,\mathrm{hole}} &= R_h \times 10^{26}\ \mathrm{cm}^{-3},\\
\langle 1/r^3\rangle_{3p\,\mathrm{electron}} &= R_e \times 10^{26}\ \mathrm{cm}^{-3}.
\end{aligned}$$

Equation (6) provides quantitative expressions for the contributions of the different parameters to the A's and B's. Estimates of a_{4s} and R_e can be obtained from the fs energy levels using formulas in Kopfermann.[15] The uncertainties in these calculations are of the order of 10%, but the uncertainties they introduce into $A(2s_2)$, $A(2p_4)$, and $B(2p_4)$ are much smaller, on the order of 1%. This is so because R_e is less than 1% as large as R_h and, as will be seen below, the a_{4s} term in Eq. (6) contributes less than 10% to $A(2s_2)$.

The preceding discussion indicates that the single dominant influence in determining each hyperfine-interaction constant is $\langle 1/r^3\rangle_{2p\,\mathrm{hole}}$. Because of the sensitivity of our expressions to this parameter, we must provide for its variation with the state of the excited electron. Equations (5) and (6) can be modified in a straightforward way to include such effects. The B of each level is less than 10% of the corresponding A in magnitude, so that small changes in $\langle 1/r^3\rangle_{2p\,\mathrm{hole}}$ have negligible influence on the hfs through the B's. (This assertion is borne out in our computer fits to the data.) But these modifications cannot be ignored in the A's. The A's from Eq. (6) are therefore written:

$$\begin{aligned}
A(2s_2) &= 0.460\,a_{4s} - 843.27R_h\,(2s_2),\\
A(2p_4) &= -228.78R_h\,(2p_4) - 251.39R_e,\\
A(1s_4) &= -54.639 - 459.74R_h\,(1s_4).
\end{aligned} \tag{7}$$

DATA ANALYSIS AND THEORETICAL FIT

Figure 4 shows typical experimental spectra, taken with the Fabry-Perot interferometer, and the computer-generated fit for forward [Fig. 4(a)] and backward [Fig. 4(b)] runs. In each case the upper experimental trace shows the narrow change signals, and the lower trace shows the Doppler-broadened background observed without the lock-in amplifier. Note that the hyperfine structure is ordinarily completely masked by the Doppler widths.

The laser frequency, which was carefully moni-

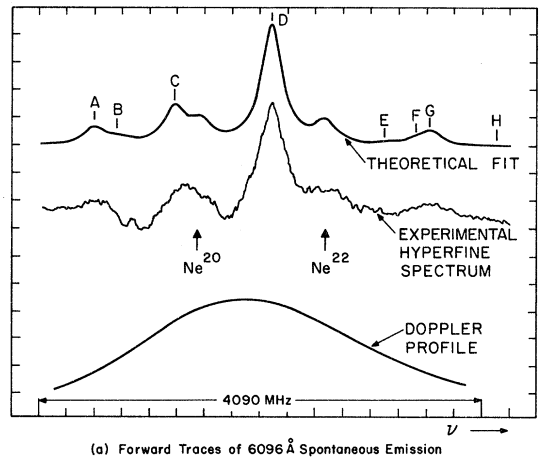

(a) Forward Traces of 6096 Å Spontaneous Emission

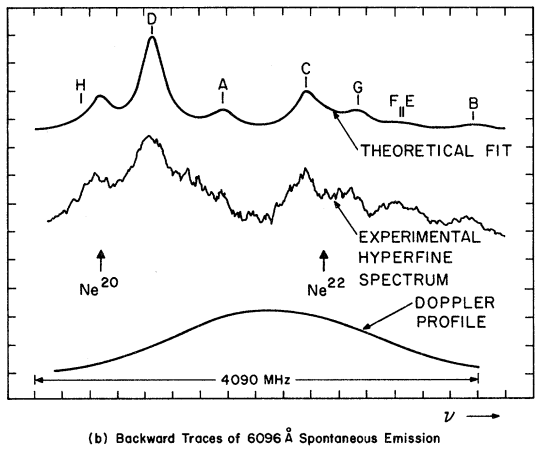

(b) Backward Traces of 6096 Å Spontaneous Emission

FIG. 4. Comparison of experimental traces and theoretical fit. Note that the Doppler profiles for forward and backward traces completely mask the hyperfine structure. The change signals labeled are the eight most prominent and are associated with three-level cascade systems of the type $F \rightarrow F' \rightarrow F''$. Denoting these systems as ordered triplets, they are $A = (\frac{3}{2}, \frac{3}{2}, \frac{1}{2})$; $B = (\frac{3}{2}, \frac{5}{2}, \frac{5}{2})$; $C = (\frac{3}{2}, \frac{3}{2}, \frac{3}{2})$; $D = (\frac{5}{2}, \frac{7}{2}, \frac{5}{2})$; $E = (\frac{5}{2}, \frac{5}{2}, \frac{3}{2})$; $F = (\frac{1}{2}, \frac{1}{2}, \frac{1}{2})$; $G = (\frac{3}{2}, \frac{5}{2}, \frac{3}{2})$; $H = (\frac{5}{2}, \frac{5}{2}, \frac{5}{2})$. For these computer fits to the data we have $\gamma_F = 265$ MHz and $\gamma_B = 225$ MHz. Of these widths ~100 MHz is instrumental; also, the Doppler width $k_1 u = 2500$ MHz.

tored, was stable to about 2 MHz over the course of a run (about 1 min). This figure is considerably smaller than the linewidths of the observed change signals, which are of the order of 250 MHz (including a Fabry-Perot width of ~ 100 MHz). The largest change signals in Fig. 4 have intensities of about 0.5% of the intensity of the spontaneous emission background. It must be emphasized that the observed spectra are richer than ordinary 6096-Å hyperfine spectra in that our data contain information about both the laser transition *and* the coupled spontaneous emission transition. The markings on Fig. 4 denote the eight three-level systems producing the observed change signals (the contribution of the remaining ten change signals being negligible). The two additional features in the forward and backward traces are due to the presence of Ne^{20} and Ne^{22} in the sample of Ne^{21}.[20]

A PDP-12 computer was used to display intensity patterns employing the expressions in Eqs. (1) and (2) and the Appendix. Trial values for the A's and B's were obtained from Eq. (6), using Fermi-Segre estimates for a_{4s} and $\langle 1/r^3 \rangle_{3p}$ and an optimum value of $\langle 1/r^3 \rangle_{2p\,\mathrm{hole}}$. Only small deviations from these trial values were required to find the hyperfine constants that provided the best fit to the data. These small deviations from the values generated from Eq. (6) can be associated with the theoretical considerations which led to Eq. (7), where a slightly different $\langle 1/r^3 \rangle_{2p\,\mathrm{hole}}$ characterizes each A.

The $\alpha(j)$'s and $\beta(j)$'s appearing in the intensity formula (Appendix), which determine the relative intensities of the change signals, were calculated from the electric dipole matrix elements.[13] A convenient simplification is that the $\alpha(j)$'s and $\beta(j)$'s are independent of the admixture of the LS wave functions for a particular fs energy level (aside from a proportionality constant).

Sixty-six runs were analyzed in all: 41 forward and 25 backward. In analyzing the data we operated under the strict requirement, imposed by the theory of laser-induced line narrowing, that the same set of A and B values has to fit both forward and backward experimental traces.

In several experimental runs, the laser frequency was intentionally shifted ~100 MHz. This alters the intensity pattern in prescribed ways (Appendix), serving as a further check on our identification of the features.

RESULTS AND DISCUSSION

The best fit to the data (Table I) provides the values: $R_h(1s_4) = 0.865 \pm 0.015$; $R_h(2p_4) = 0.948 \pm 0.013$; $R_h(2s_2) = 0.866 \pm 0.020$. The slightly larger error in the latter value is due to the uncertainty in estimating a_{4s}.

Combining $\langle 1/r^3 \rangle_{2p\,\mathrm{hole}}$ for the $1s_4$ level with $B(1s_5)$ from Ref. 16, we obtain an accurate value for the uncorrected nuclear quadrupole moment $Q(1s)$ of Ne^{21}: $Q(1s) = (0.0926 \pm 0.0016)$ b. This is in good agreement with the value quoted in Ref. 16. Estimates of Q for the other two levels would be less accurate since our experiment is not very sensitive to the precise values of the corresponding B's.

To establish the actual nuclear quadrupole moment Q_0, corrections for shielding and antishielding effects must be taken into account.[21,22] For the $2p^5$ configuration of the neon core, the Sternheimer correction factor R has been estimated to be[23,24] $R \approx 0.10 \pm 0.05$, where $Q_0 = Q/(1-R)$. Thus

$$Q_0 = \frac{(0.0926 \pm 0.0016)\,\mathrm{b}}{0.90 \pm 0.05} = (0.1029 \pm 0.0075)\,\mathrm{b}$$

for the corrected value of the quadrupole moment of Ne^{21}.

We can also obtain a value for a_{3s}, the Fermi contact interaction constant, from Eq. (5) and our value of $\langle 1/r^3\rangle_{2p\ \mathrm{hole}}$ for the $1s_4$ level (Table I). Note that this value is 15% smaller in magnitude than that calculated from the Fermi-Segre formula.

Our values of $\langle 1/r^3\rangle_{2p\ \mathrm{hole}}$ for the $2s_2$ and $1s_4$ levels, which have the excited electron in an s state, are within 1% of each other. The corresponding result for the $2p_4$ level is about 10% larger than these. The former two values are in close agreement with the semiempirical value for the $1s_5$ level from Ref. 16.

It is interesting to compare these values with that for the neon-ion ground state, in which the excited electron surrounding the $2p$ hole is removed. A calculation using restricted Hartree-Fock wave functions[25] gives a value for $\langle 1/r^3\rangle_{2p\ \mathrm{hole}}$ which is within 2% of our results for the $2s_2$ and $1s_4$ levels.

These conclusions are, of course, subject to the approximations made in deriving the A's of Eq. (7) and the B's of Eq. (6). One source of error is the uncertainty in the LS admixture coefficients of our wave functions [Eq. (4)]. These values are expected to be accurate for the $1s_4$ and $2s_2$ levels, but somewhat less certain for the $2p_4$ level. This is primarily due to the difficulties associated with properly including effects from spin-spin and spin-other-orbit interactions.[26] Note that the value of $A(2p_4)$ is particularly sensitive to small deviations in the admixture coefficients, since the $2p_4$ state is ~89% a pure $|{}^3P_2\rangle$ state.

The assumption of a single $\langle 1/r^3\rangle_{2p\ \mathrm{hole}}$ characterizing each level ignores core-polarization effects,[27] which result from the spin-dependent distortion of the $(1s)^2$ $(2s)^2$ core by the outer electrons. Taking this effect into account theoretically would necessitate for each level: (i) the use of different values of $\langle 1/r^3\rangle_{2p\ \mathrm{hole}}$ in the magnetic hfs resulting from the orbital and spin moments of the electrons; (ii) a separate value of $\langle 1/r^3\rangle_{2p\ \mathrm{hole}}$ associated with the quadrupole interaction; and (iii) would also add a small contact term to the expressions for the A's.

It should be possible to explore fully the details of the above considerations by studying the laser-induced change signals produced at other transitions branching from the upper and lower levels of the 1.15 μ and other neon laser lines.

We have also measured the $Ne^{20,21,22}$ isotope shifts at 1.15 μ and 6096 Å. Ne^{20} and Ne^{22} were introduced into the sample cell containing Ne^{21} to bring up the intensities of their change signals, thus facilitating their identification and measurement. The shifts for the 1.15-μ and 6096-Å transitions are extracted from the change-signal spectra using Eq. (3) [and Eq. (1) in the case of Ne^{21}], and are summarized in Table II. The $Ne^{20,22}$ results are in excellent agreement with previously measured values.[2,28,29] Note in particular that the 1.15-μ transition of Ne^{21} is shifted to a higher frequency than that of Ne^{22}. Similar inversions in isotopic order have been reported in xenon.[30] Such inversions demonstrate deviations from simple mass-effect considerations in the isotope shifts. An analysis of the results is in progress and will be reported later.

CONCLUSION

We have demonstrated the applicability of laser-

TABLE I. Experimental results for hyperfine interaction constants and values for $\langle 1/r^3\rangle_{2p\ \mathrm{hole}}$, Q', and a_{3s}.

	Ne^{21} fs levels		
	$1s_4$	$2p_4$	$2s_2$
Magnetic dipole hyperfine interaction constant A (MHz)	-452 ± 7	-219 ± 3	-756 ± 15
Electric quadrupole hyperfine interaction constant B (MHz)[a]	$+44$	$+15$	-39
R_h (where $\langle 1/r^3\rangle_{2p\ \mathrm{hole}}=R_h\times10^{26}$ cm^{-3})	0.865 ± 0.015	0.948 ± 0.013	0.866 ± 0.020

(In each case the quoted error includes at least 70% of the data points.)

Nuclear quadrupole moment Q: $Q(1s_4$[a]$=(0.0926\pm0.0016)$b $[Q(1s_5)$[b]$=(0.093\pm0.010)$ b]

Corrected value Q_0: Q_0[c] $=(0.1029\pm0.0075)$ b

Fermi contact term for 3s electron: $a_{3s}=-207$ MHz $[a_{3s}$[d]$=-245$ MHz]

$\langle 1/r^3\rangle_{2p\ \mathrm{hole}}$ comparison of different configurations: $R_h(1s_4)=0.865\pm0.015$ $[R_h(1s_5)$[e]$=0.86\pm0.09]$ $[R_h(\mathrm{Ne}^+)$[f]$=0.84]$

[a]Obtained from the value of $B(1s_5)$ of Ref. 16 and the coupling formulas Eq. (5).
[b]Reference 16.
[c]References 23 and 24.
[d]Fermi-Segre estimate.
[e]Semiempirical value derived from Ref. 16.
[f]Calculated in Ref. 25.

TABLE II. Observed isotope shifts at 6096 Å and 1.15 μ in $Ne^{20,21,22}$ (in MHz).

	$\nu(Ne^{22})-\nu(Ne^{20})$				$\nu(Ne^{22})-\nu(Ne^{21})$
	Present work	Reference 2	Reference 28	Reference 29	Present work
6096 Å	1708 ± 26	1706 ± 30	1680 ± 30	···	1010 ± 30
1.15 μ	261 ± 5	257 ± 8	···	261 ± 3	−186 ± 6

induced line-narrowing techniques in observing optical hfs in a system whose features are ordinarily masked by Doppler broadening. These techniques can be applied in principle to measurements of closely spaced structure of transitions coupled directly or indirectly through radiative cascade to either of the laser levels.

Although the change signals in this experiment are considerably narrower than the Doppler width, for many other systems they may be two or three orders of magnitude narrower still. The limits on the resolution are only determined by the homogeneous width of the lines and the resolution of the detection apparatus.

ACKNOWLEDGMENTS

The authors would like to thank Professor Norman Kurnit, Professor Abraham Szöke, and Philip Mongeau for their contributions to the progress of this experiment. Helpful discussions with Professor George Koster are gratefully acknowledged.

APPENDIX: THEORETICAL EXPRESSION FOR INTENSITY PATTERNS OF CHANGE SIGNAL (SEE FIG. 4)

The following expression is derived from Eq. (58) of Ref. 1:

$$I_{F,B}=\sum_j \exp\left[-\left(\frac{\Omega_1-\omega_1(j)}{k_1 u}\right)^2\right]\left\{c_1 \sum_{M_{F'},M_{F''}} |\alpha(j)|^2 + c_2 \sum_{M_F,M_{F'},M_{F''}} |\alpha(j)|^2|\beta(j)|^2 \Big/ \left[1+\left(\frac{\Omega_1-\Omega_{F,B}(j)}{\Gamma_{F,B}/2}\right)^2\right]\right\},$$

where $\sum_j$ refers to the sum over all possible cascade transitions of the type $F \to F' \to F''$.

For the laser field polarized in the z direction and propagating along the y axis,

$$|\alpha(j)|^2 = |\mu_x(F', M_{F'}; F'', M_{F''})|^2 + |\mu_z(F', M_{F'}; F'', M_{F''})|^2$$

(for observation of both polarizations of the 6096-Å radiation together),

$$|\beta(j)|^2 = |\mu_z(F, M_F; F', M_{F'})|^2;$$

μ's are the hyperfine electric dipole matrix elements and can be obtained from tables in Ref. 13.

Note that the relative magnitudes of the $\alpha(j)$'s and $\beta(j)$'s are independent of the fs coupling of the levels. Ω_1 is the frequency of the spontaneous emission at 6096 Å. $\Omega_{F,B}$ are defined in the text. Explicit expressions for the proportionality constants c_1 and c_2 are given in Ref. 1.

The linewidths of the change signals (full width at half-maximum) are

$$\gamma_{F,B}=\gamma_1+[(\omega_1/\omega_2)(\gamma_0+\gamma_2)\pm\gamma_0],$$

where γ_i is the decay rate of level i. For our case $i=0$, 1, 2 correspond to the $2p_4$, $1s_4$, and $2s_2$ levels, respectively (see Ref. 1 for details).

*Work supported by Air Force Cambridge Research Laboratories and National Aeronautics and Space Administration.

[1] M. S. Feld and A. Javan, Phys. Rev. 177, 540 (1969). Other references may be found in this paper.

[2] R. H. Cordover, P. Bonczyk, and A. Javan, Phys. Rev. Letters 18, 730 (1967).

[3] W. G. Schweitzer, M. M. Birkey, and J. A. White, J. Opt. Sci. Am. 57, 1226 (1967).

[4] H. K. Holt, Phys. Rev. Letters 20, 410 (1968).

[5] In previous experiments (Refs. 2–4), done within the laser resonator, the forward and backward signals appear together. This standing-wave configuration makes the analysis of the complex spectra much more difficult than does a running-wave experiment which separates forward and backward spectra.

[6] The Paschen designation of the levels is used. The corresponding configurations are $2s_2: 2p^5(^2P_{1/2}^\circ)4s(J=1)$, $2p_4: 2p^5(^2P_{1/2}^\circ)3p(J=2)$, $1s_4: 2p^5(^2P_{3/2}^\circ)\ 3s(J=1)$. For notation, see C. E. Moore, *Atomic Energy Levels*, National Bureau of Standards, Circular No. 467 (U.S. GPO, Washington, D. C., 1949), Vol. 1.

[7] The linewidth of the change signal (full width at half-maximum) in the forward (backward) direction, is given by

$$\gamma_{F,B}=\gamma_1+[(\omega_1/\omega_2)(\gamma_0+\gamma_2)\pm\gamma_0],$$

where γ_j is the decay rate of level j. See Ref. 1 for details.

[8] P. H. Lee, P. B. Schoefer, and W. B. Barker, Appl. Phys. Letters 13, 373 (1968); M. S. Feld, A. Javan, and P. H. Lee, *ibid.* 13, 424 (1968).

[9] I. M. Beterov and V. P. Chebotaev, Zh. Eksperim. i Teor. Phys. Pis'ma v Redaktisyu 9, 216 (1969) [Sov. Phys. JETP Letters 9, 127 (1969)].

[10] In the backward runs the 6096-Å fluorescence is taken from the sample cell by means of a mirror placed near the entrance window at 45° (Fig. 3). The laser beam enters the cell through a small hole in the mirror.

[11]D. H. Rank and J. N. Shearer, J. Opt. Sci. Am. 46, 463 (1956).
[12]The fs energy levels were obtained from Ref. 6, p. 77.
[13]E. U. Condon and G. H. Shortley, *The Theory of Atomic Spectra* (Cambridge U. P., London, 1959).
[14]L. A. Vainshtein and L. A. Minaeva, Ah. Priklad. Spektrosk. (USSR) 8, 244 (1968).
[15]H. Kopfermann, *Nuclear Moments*, (Academic, New York, 1958).
[16]G. M. Grosof, P. Buck, W. Lichten, and I. I. Rabi, Phys. Rev. Letters 1, 214 (1958).
[17]J. T. Latourrette, W. E. Quinn, and N. F. Ramsey, Phys. Rev. 107, 1202 (1957).
[18]W. J. Childs, Phys. Rev. A 2, 316 (1970).
[19]Kopfermann (Ref. 15) gives expressions for sp and pp' magnetic dipole matrix elements and sp electric quadrupole matrix elements. The latter formula, first given by Casimir [H. Casimir, Teylors Tweede Genootshap 11, 255 (1936)] is inconsistent with the matrix elements in Ref. 16, and appears to be in error. The "12" in the third term on the right-hand side of Ref. 15, Eq. (31.4), should be a "6." We wish to thank W. J. Childs for his helpful comments and for pointing this out.
[20]The isotopic mixture of the Ne^{21} sample used was 87.9% Ne^{21}; 10.2% Ne^{20}; 1.9% Ne^{22}.
[21]R. M. Sternheimer, Phys. Rev. 84, 244 (1951).
[22]R. M. Sternheimer, Phys. Rev. 164, 10 (1967).
[23]R. M. Sternheimer and R. F. Peierls, Phys. Rev. A 4, 1722 (1971).
[24]R. M. Sternheimer (private communication). We are grateful to Dr. Sternheimer for providing us with the results of his calculation.
[25]H. F. Schaefer, III and R. A. Klemm, Phys. Rev. A 1, 1063 (1970).
[26]Calculations of the LS admixture coefficients based on the fs energy splittings, including only spin-orbit and electrostatic interactions, are in excellent (0.1%) agreement with the values quoted in Ref. 14 [Eq. (4)] for the $1s_4$ and $2s_2$ levels. For the $2p_4$ level, there is a difference of ~5% in the coefficient of the dominant $|^3P_2\rangle$ basis state.
[27]See for example, B. G. Wybourne, *Spectroscopic Properties of Rare Earths* (Interscience, New York, 1967).
[28]H. Nagaoka and T. Mishima, Institute Phys. Chem. Research (Tokyo) 13, 293 (1930).
[29]A. Szöke and A. Javan, Phys. Rev. Letters 10, 521 (1963).
[30]D. A. Jackson and M. C. Coulombe, Compt. Rend. B268, 146 (1969).

PHYSICAL REVIEW A VOLUME 5, NUMBER 3 MARCH 1972

Atomic M-Shell Coster-Kronig, Auger, and Radiative Rates, and Fluorescence Yields for Ca–Th†

Eugene J. McGuire
Sandia Laboratories, Albuquerque, New Mexico 87115
(Received 20 October 1971)

Calculated Auger, Coster-Kronig, super Coster-Kronig, and radiative transition rates are used to compute atomic M-shell Auger, Coster-Kronig, and fluorescence yields. Comparison is made with five fluorescence-field measurements, with full width at half-maximum measurements of L-M x rays, and with Bhalla's relativistic radiative-yield calculations.

I. INTRODUCTION

Little experimental information is available on atomic decay schemes for the M shell.[1] Yet such information is useful in interpreting L-M x-ray transition half-widths, surface studies based on Auger electron emission, studies of M-shell photoabsorption, studies of final charge states following inner-shell ionization, etc. The present author has shown, semiquantitatively, how strongly the lifetime of a $3p$ hole affects the photoabsorption cross section in the solids Ti to Co.[2] In this paper, in addition to comparing calculated and measured mean M-shell fluorescence yields, measured and calculated L-M x-ray half-widths are compared. In succeeding papers we will examine detailed Auger electron emission spectra following ionization of the M shell,[3] and study final-charge-state production following ionization of the K, L, and M shell for the elements up to Kr.[4] However, it must be emphasized that there is little experimental information available on such gross quantities as fluorescence yields, and none available on Coster-Kronig yields. Thus, the reliability of these results is something of an open question.

II. CALCULATED TRANSITION RATES

Before outlining the procedures used in the calculation we need to supplement the definitions of yields used in the case of L-shell decay.[1] The need arises because in the M shell for $Z \leq 36$ there exists the possibility that $3s$ and $3p$ holes can decay with the creation of two other M-shell holes. These have been called super Coster-Kronig transitions.[2] Paralleling the definitions used in L-shell decay we define ω_{M_i} as the probability that an M_i-subshell hole will decay by a radiative transition from a higher shell, but not from a higher M subshell (these latter transitions are negligibly weak but are included in the definition of the Coster-Kronig yield). We define a_{M_i} as the probability that an M_i-subshell hole